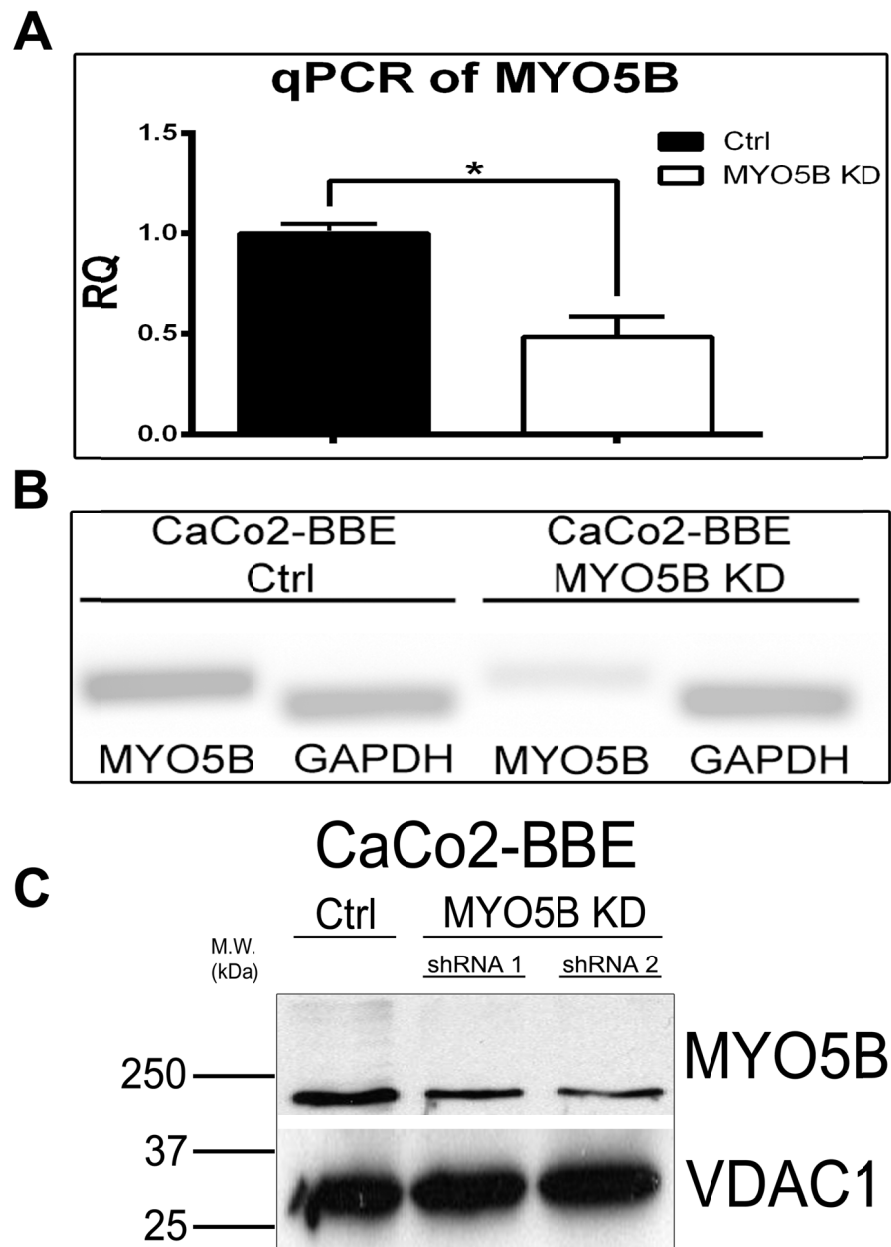
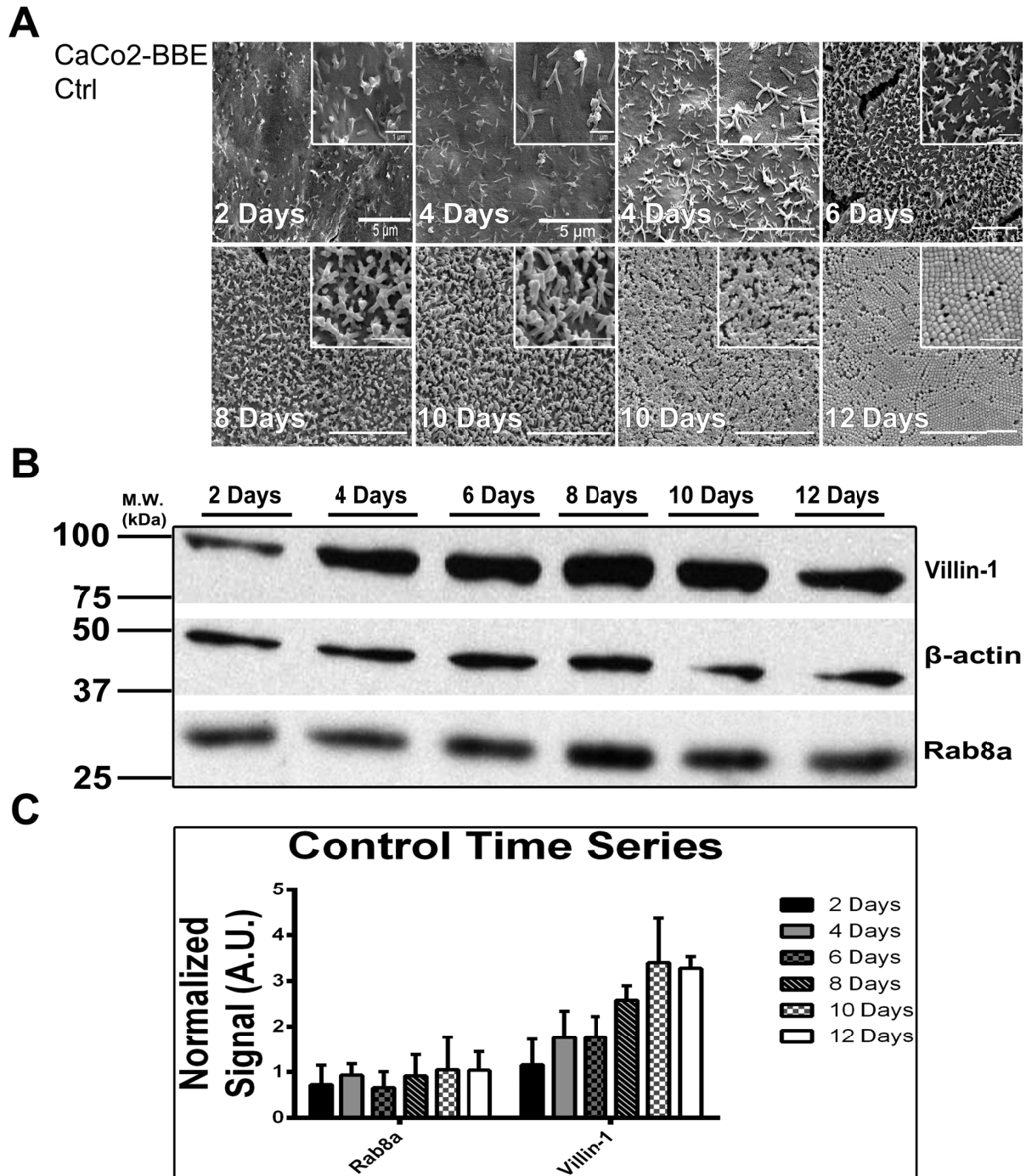


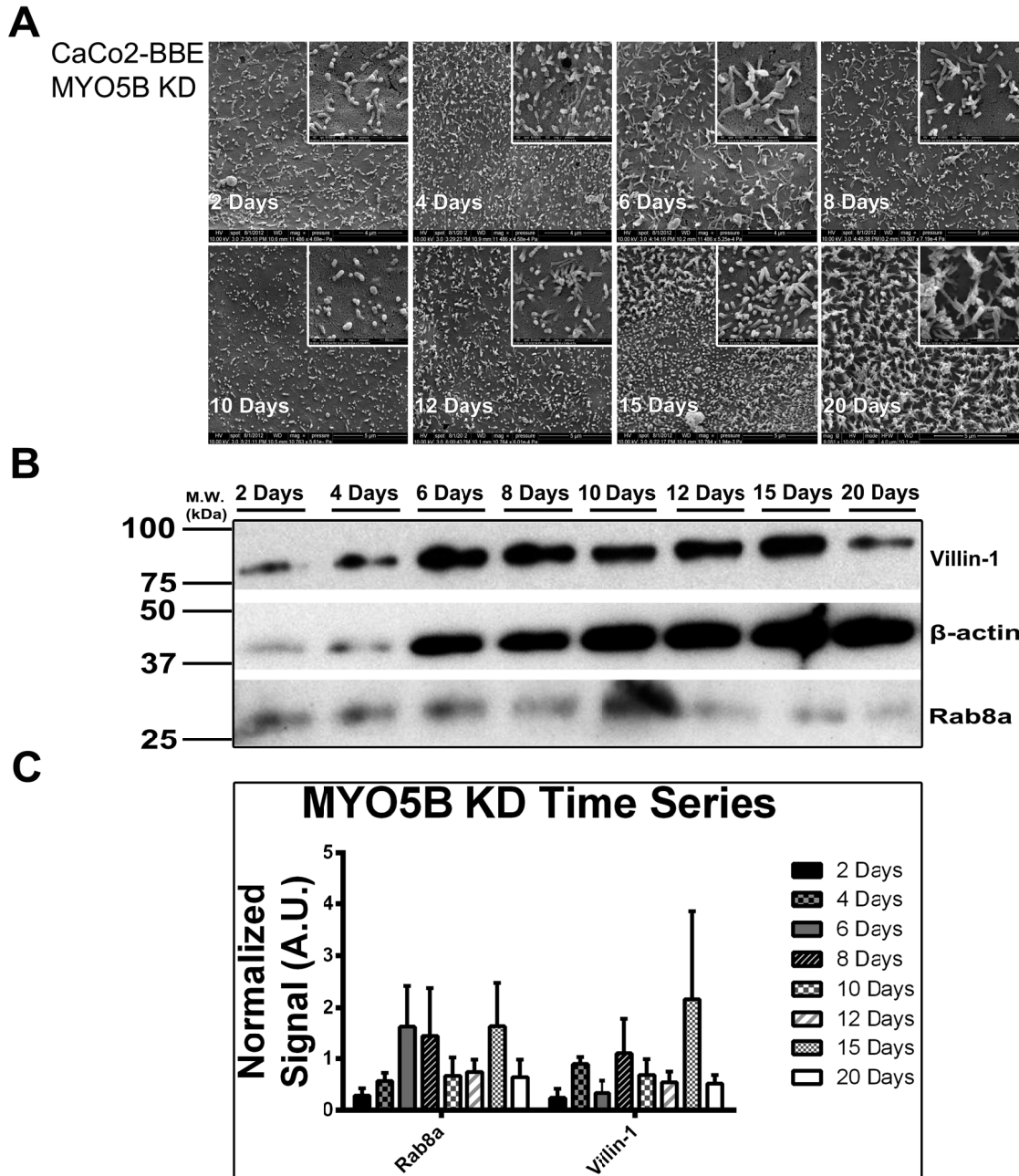
Supplemental Figures



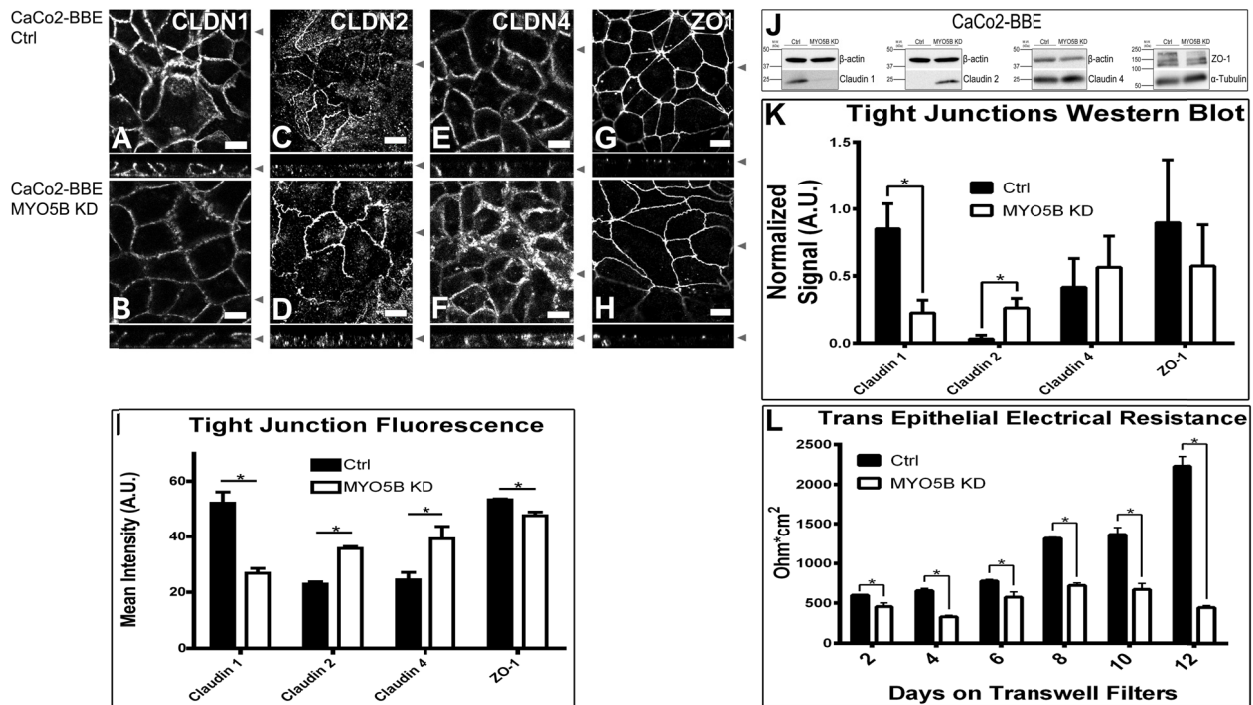
Supplemental Figure 1. In CaCo2-BBE MYO5B-KD cells MYO5B expression is significantly reduced. (A) Real Time-PCR shows a 50% reduction of MYO5B in CaCo2-BBE MYO5B-KD shRNA 2 cell line. (B) Reverse Transcription-PCR shows a reduction of MYO5B in CaCo2-BBE MYO5B-KD shRNA 2 cell line. (C) Western blot of CaCo2-BBE control and MYO5B-KD shRNA 1 and shRNA 2 cell lines probed for MYO5B and VDAC1, as a control, showing a reduction of MYO5B protein expression. Statistical significance is denoted by * $p \leq 0.05$, ** $p \leq 0.01$, and *** $p \leq 0.001$ using the Mann-Whitney-test. Error bars denote S.E.M.



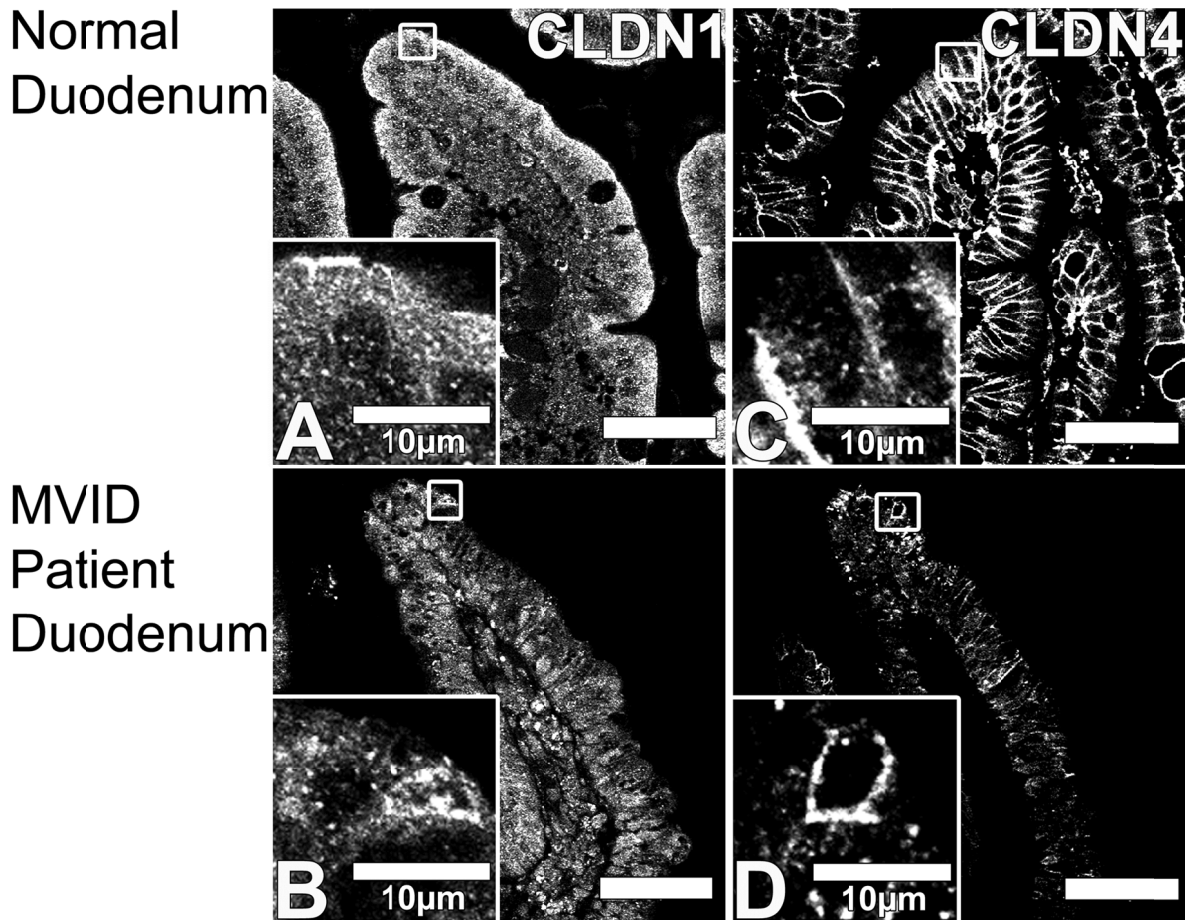
Supplemental Figure 2. Scanning electron micrographs and western blots of control CaCo2-BBE cells in a time series from 2 to 12 days on transwells. (A) SEM images of cells cultured from 2 to 12 days on transwells illustrate the progression of microvilli development with insets at higher magnifications. Note, the progression of microvillar packing in CaCo2-BBE control cells becomes more complex over time. Scale bars are 5 μ m in the panels and 1 μ m in the insets. (B and C) Western blots with quantitation of villin-1, β -actin, and Rab8a showing that villin-1 is up-regulated throughout microvillar development.



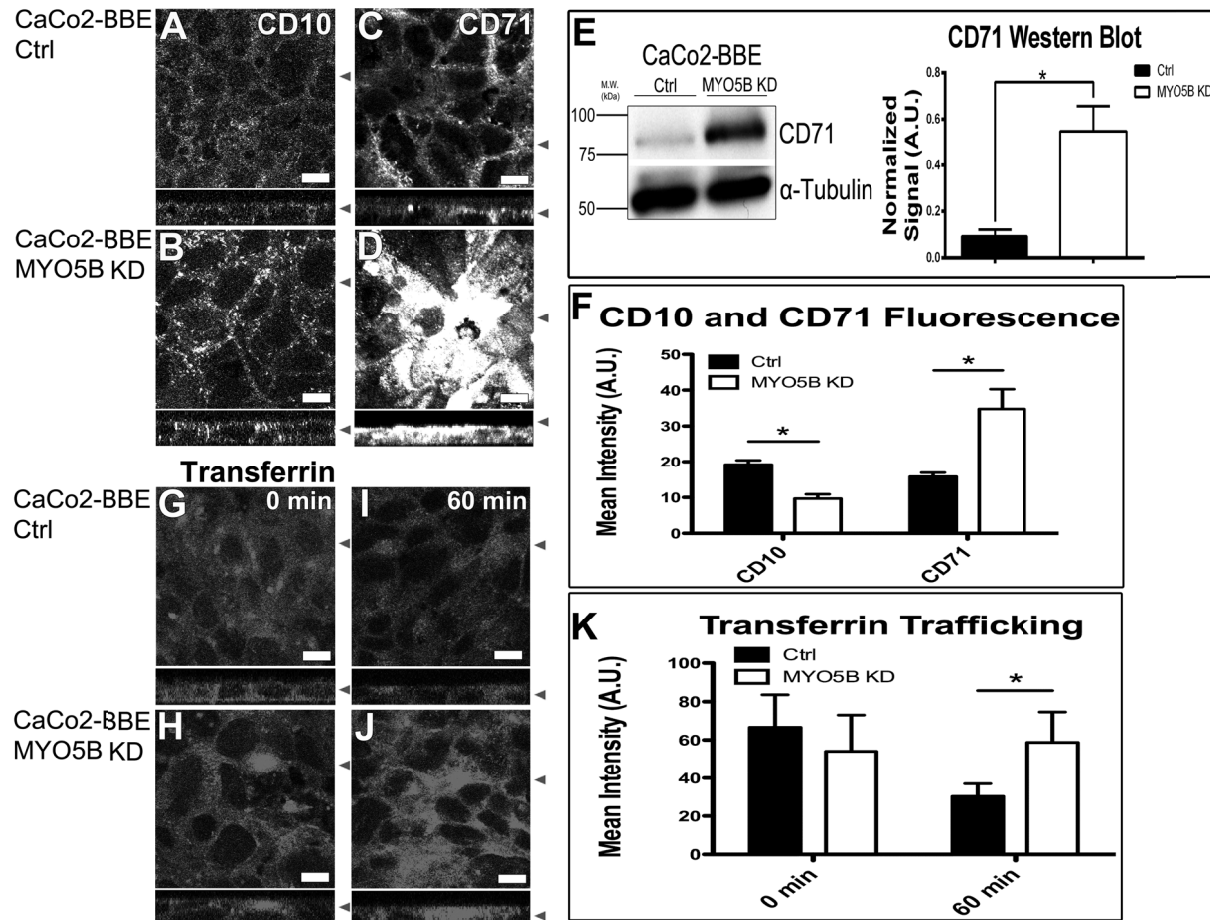
Supplemental Figure 3. Scanning electron micrographs and western blots of MYO5B-KD CaCo2-BBE cells in a time series from 2 to 20 days on transwells. (A) SEM images of cells grown on transwells from 2 to 20 days illustrate the progression of microvilli development with insets at higher magnifications. Note, that microvillar packing is never fully established. Scale bars in panels denoting days 2, 4, and 6 are 4 μ m and 1 μ m in the panel and its inset, respectively, except the panel denoting the inset for day 6, in which it is 500nm. Scale bars in all other panels are 5 μ m and 1 μ m in all panels and insets, respectively, except the inset for day 10, in which it is 500nm. (B and C) Western blots with quantitation of villin-1 and Rab8a that show no up-regulation of villin-1 throughout microvillar development until the 20 day time point.



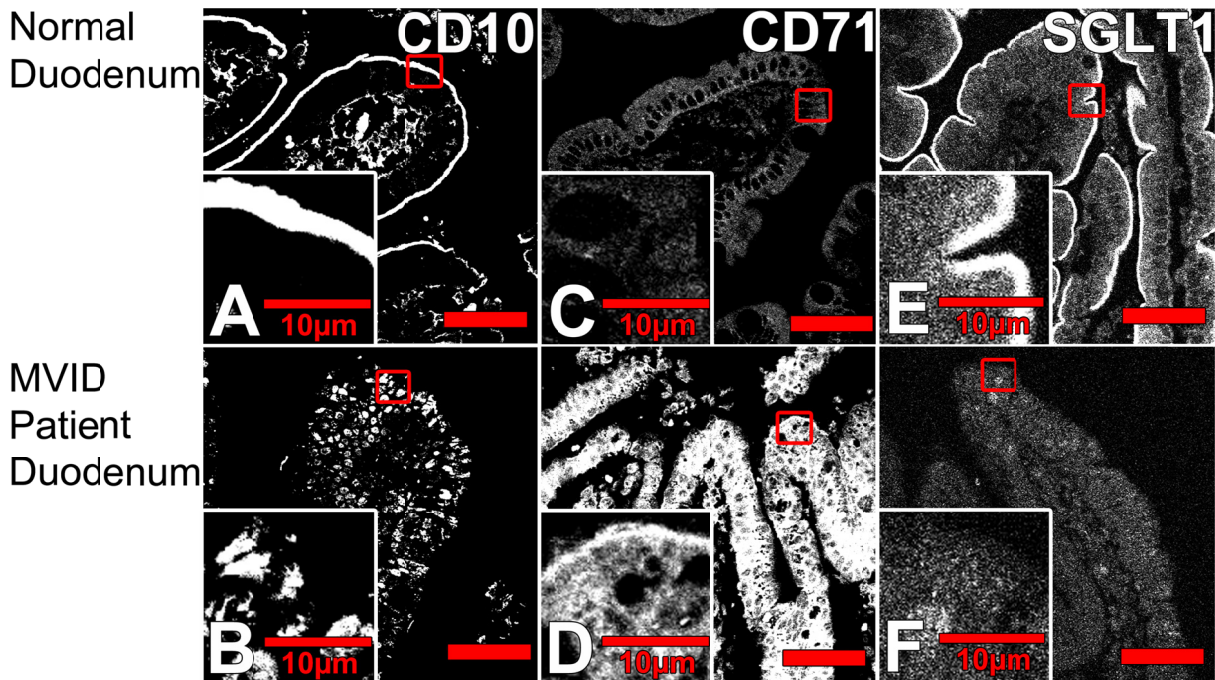
Supplemental Figure 4. Junctional compartment immunofluorescence staining in CaCo2-BBE MYO5B-KD cells shows a shift in claudin staining. In panels A-H, X-Y confocal images are shown above Z-axis reconstructions. (A-B) In control cells, CLDN1 has a lateral distribution, and in MYO5B-KD cells, CLDN1 staining is decreased but maintained a lateral distribution. (C-D) In control cells, CLDN2 has a junctional distribution, while in MYO5B-KD cells, CLDN2 staining becomes more intensely junctional than in the control cells. (E-F) In control cells, CLDN4 has a lateral distribution, and in MYO5B-KD cells, CLDN4 has a lateral cytoplasmic distribution. (G-H) In control cells, ZO-1 has a junctional distribution, and MYO5B-KD cells, ZO-1 has the same distribution as the control. (I) Quantitation of mean fluorescence of CLDN1, CLDN2, CLDN4, and ZO-1 immunofluorescence showed a reduction in CLDN1 and ZO-1 and an increase in CLDN2 and CLDN4 in MYO5B-KD cells. (J-K) Western blot analysis and quantitation of MYO5B-KD cells compared with control cells, CLDN1 was down-regulated and CLDN2 was up-regulated. It should be noted, the gel used for Rab11a in Figure 7 was stripped and re-probed for CLDN1 and CLDN2, and as a result they have the same loading controls. (L) The trans-epithelial resistance was decreased in MYO5B-KD cells. Scale bars are 10 μ m in all panels. Statistical significance is denoted by * $p \leq 0.05$, ** $p \leq 0.01$, and *** $p \leq 0.001$ using the Mann-Whitney-test. Error bars denote S.E.M.



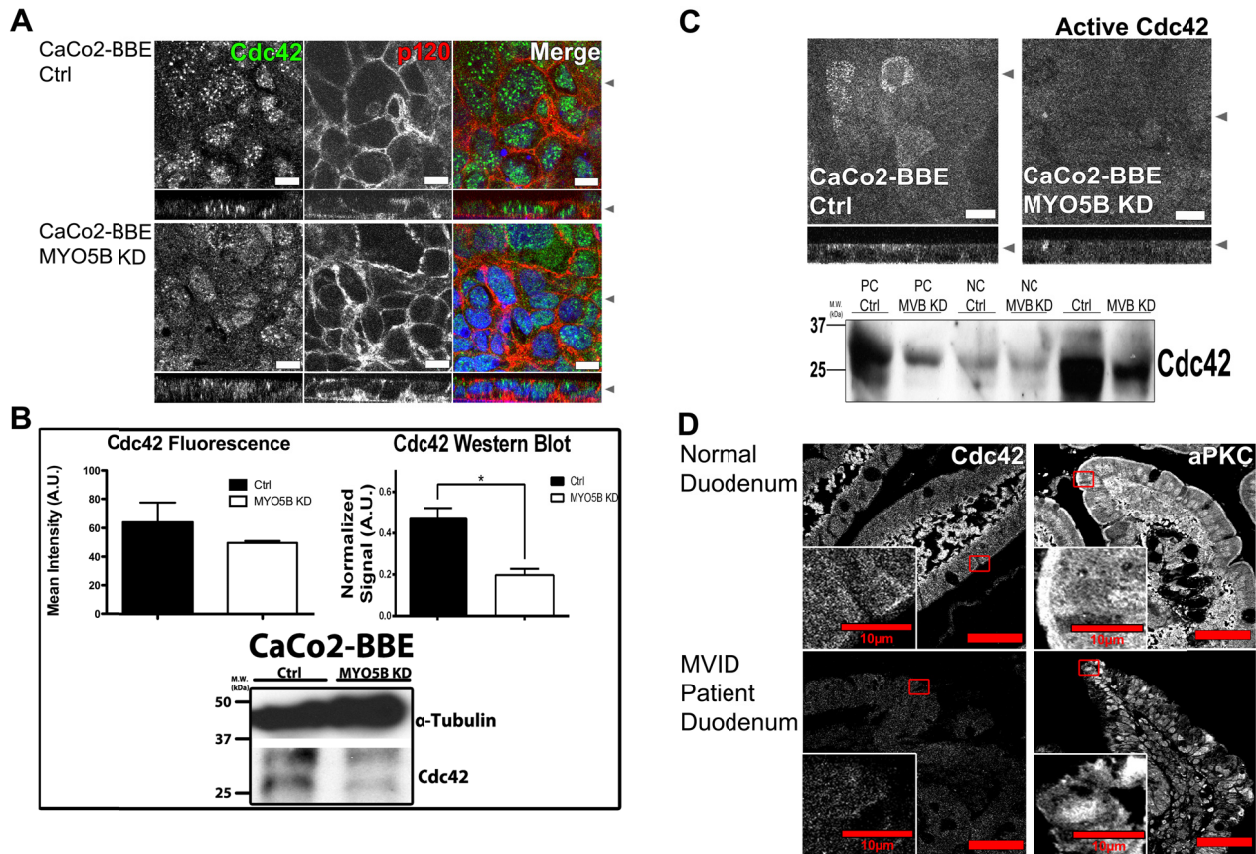
Supplemental Figure 5. Junctional compartment immunofluorescence staining in MVID patient duodenum shows alterations in claudin staining. (A-B) CLDN1 staining in normal duodenum showed a junctional distribution, while CLDN1 staining in MVID patient duodenum showed dispersal of the junction staining. (C-D) CLDN4 staining in normal duodenum showed a lateral distribution, while CLDN4 staining in MVID patient duodenum showed reduced fluorescence and lateral distribution. Scale bars are 50µm in all panels and are 10µm in all insets.



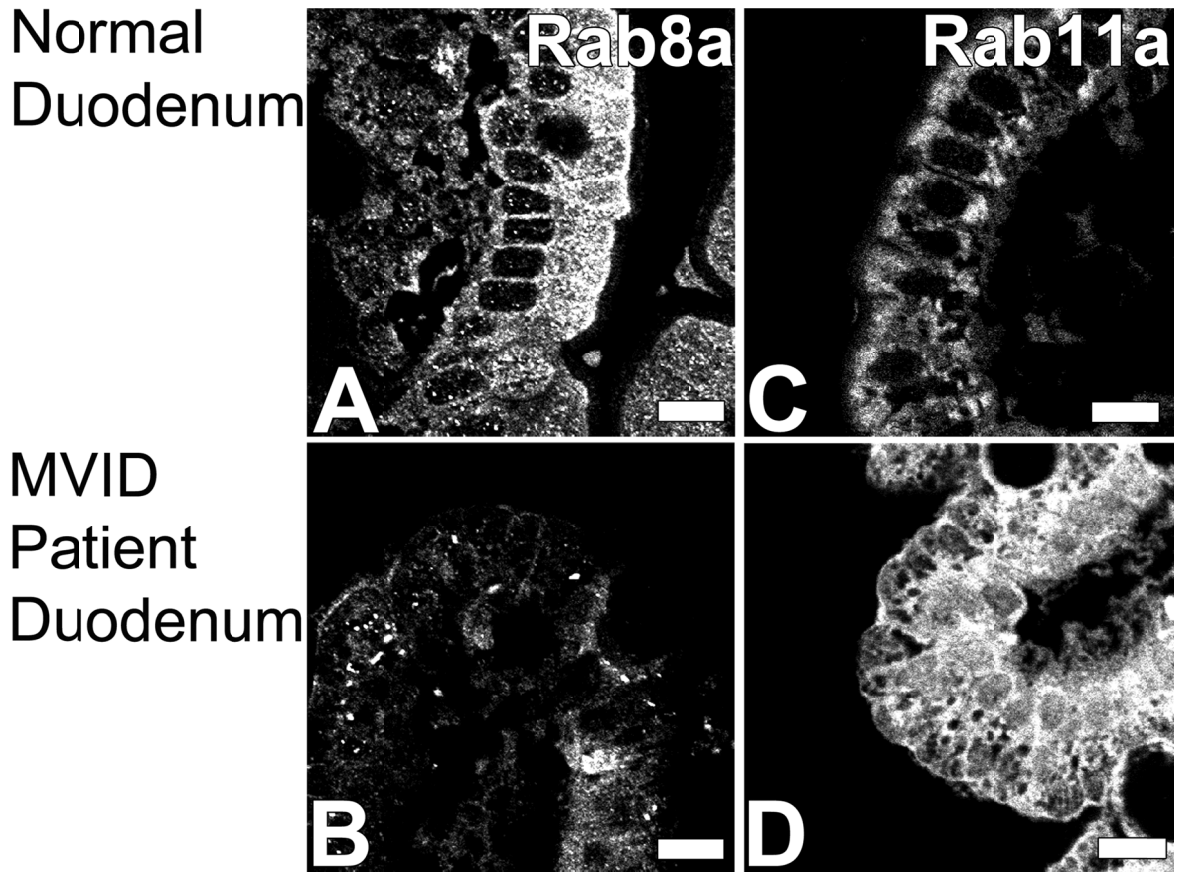
Supplemental Figure 6. Deficits in apical trafficking are observed in CaCo2-BBE MYO5B-KD cells. CD10 staining in control cells (A) was diffusely cytoplasmic and laterally distributed, while MYO5B-KD cells (B) showed concentration in both apical and lateral compartments in large punctate vesicles. In control cells (C), CD71 staining showed an apical and lateral cytoplasmic distribution, while MYO5B-KD cells (D) showed concentrated staining mainly in the sub-apical compartment with some lateral distribution. (E) Total CD71 protein was increased in MYO5B-KD cells by western blot analysis. (F) Quantitation of mean fluorescence in maximum-intensity Z-stack projections showed reduction of CD10 and increase in CD71 in MYO5B-KD cells. (G-K) Fluorescently-labeled transferrin was endocytosed from the basolateral membranes and then chased with serum for 60 minutes in both CaCo2-BBE control and MYO5B-KD cells. (G and H) Control and MYO5B-KD cells at the zero time point. (I) After 60 minutes control recycled most of the labeled transferrin out of the cells. (J) In MYO5B-KD cells fluorescently-labeled transferrin accumulated in sub-apical vesicles rather than being recycled as in control cells after 60 minutes of serum chase. (K) Quantitation of mean fluorescence in maximum-intensity Z-stack projections of transferrin showed no significant difference in uptake between the control and the MYO5B-KD cells at 0 minutes, and retention of transferrin in MYO5B-KD cells at 60 minutes. In panels (A-D and G-J), X-Y confocal images are shown above Z-axis reconstructions. Scale bars are 10µm in all panels. Statistical significance is denoted by * $p \leq 0.05$ using the Mann-Whitney-test. Error bars denote S.E.M.



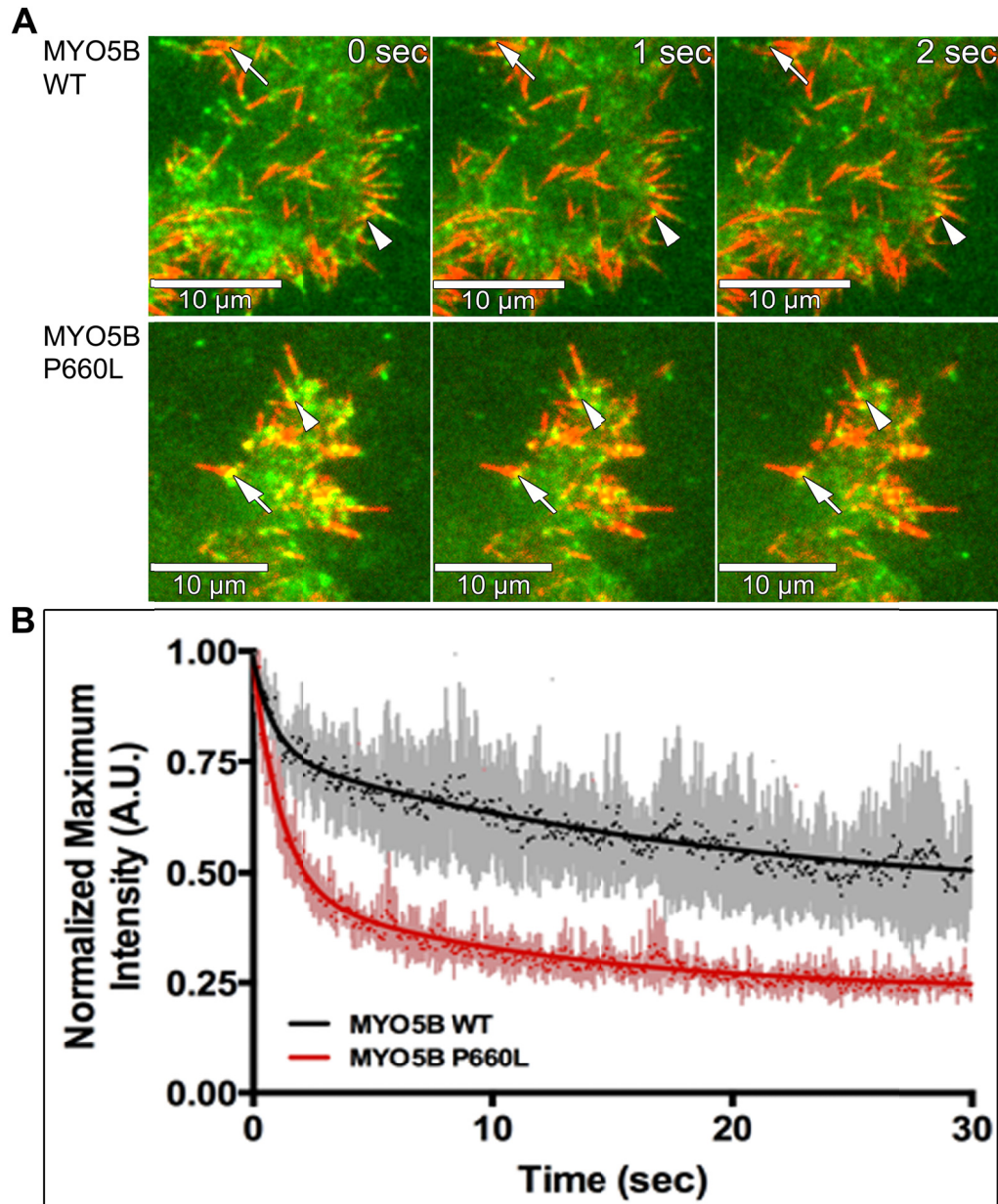
Supplemental Figure 7. MVID patient duodenum samples show redistribution of apical non-structural microvillar markers to the cytoplasm. (A) In normal duodenum, CD10 staining was localized to the brush border. (B) In MVID patient duodenum, CD10 staining was redistributed into large cytoplasmic intracellular vesicles. (C) In normal duodenum, CD71 staining was localized diffusely throughout the enterocytes. (D) In MVID patient duodenum, CD71 staining was increased and sharply redistributes to the apical surface. (E) In normal duodenum, SGLT1 was present at the apical brush border of the enterocytes. (F) In MVID patient duodenum, we observed a general loss of SGLT1 apical staining. Scale bars are 50µm in all panels and 10µm in all insets.



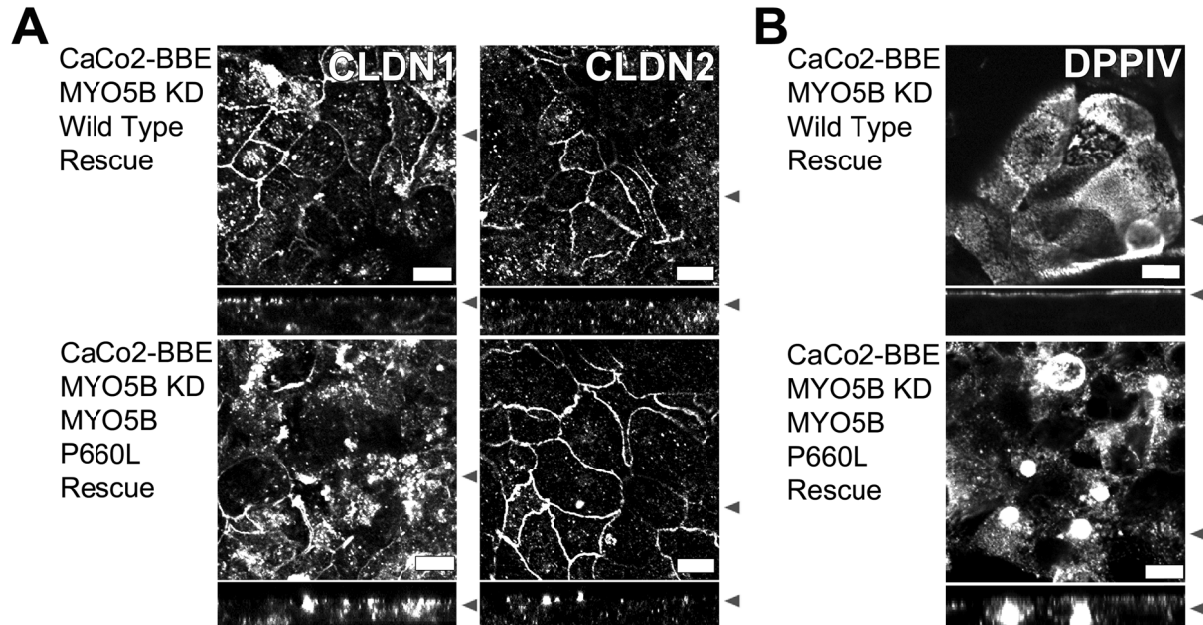
Supplemental Figure 8. Cdc42 staining in CaCo2-BBE cells and MVID patient samples demonstrated loss of total Cdc42 in MYO5B-KD. In panels A and C, X-Y confocal images are shown above Z-axis reconstructions. (A) Top: Control cells stained with Cdc42 antibodies showed two Cdc42 populations; one was dispersed throughout the cell and another existed in small discrete puncta. Bottom: MYO5B-KD cells stained with Cdc42 showed dispersal and loss of Cdc42. (B) Top-Left: Quantitation of mean fluorescence in maximum-intensity Z-stack projections of Cdc42 fluorescence. Top-Right: Western blot quantitation showed a decrease in total Cdc42 in MYO5B-KD. Bottom: Western blot showed a decrease in total Cdc42 in MYO5B-KD. (C) Top-Left: In control cells, active Cdc42 accumulated in sub-apical puncta by immunostaining. Top-Right: In MYO5B-KD cells, active Cdc42 was reduced by immunostaining. Bottom: Cdc42 activity assay of control and MYO5B-KD cells with GTP γ S positive controls labeled (PC) and GDP γ S negative controls labeled (NC) showed a decrease in total Cdc42 and a decrease in active Cdc42 in MYO5B-KD cells. (D) Top: In normal duodenum, Cdc42 and aPKC staining was localized to the brush border. Bottom: In MVID patient duodenum, Cdc42 was decreased and aPKC was redistributed into the cytoplasm. Scale bars in A and C are 10 μ m, and in D are 50 μ m in all panels and 10 μ m in the insets. Statistical significance is denoted by * $p \leq 0.05$, ** $p \leq 0.01$, and *** $p \leq 0.001$ using the Mann-Whitney-test. Error bars denote S.E.M.



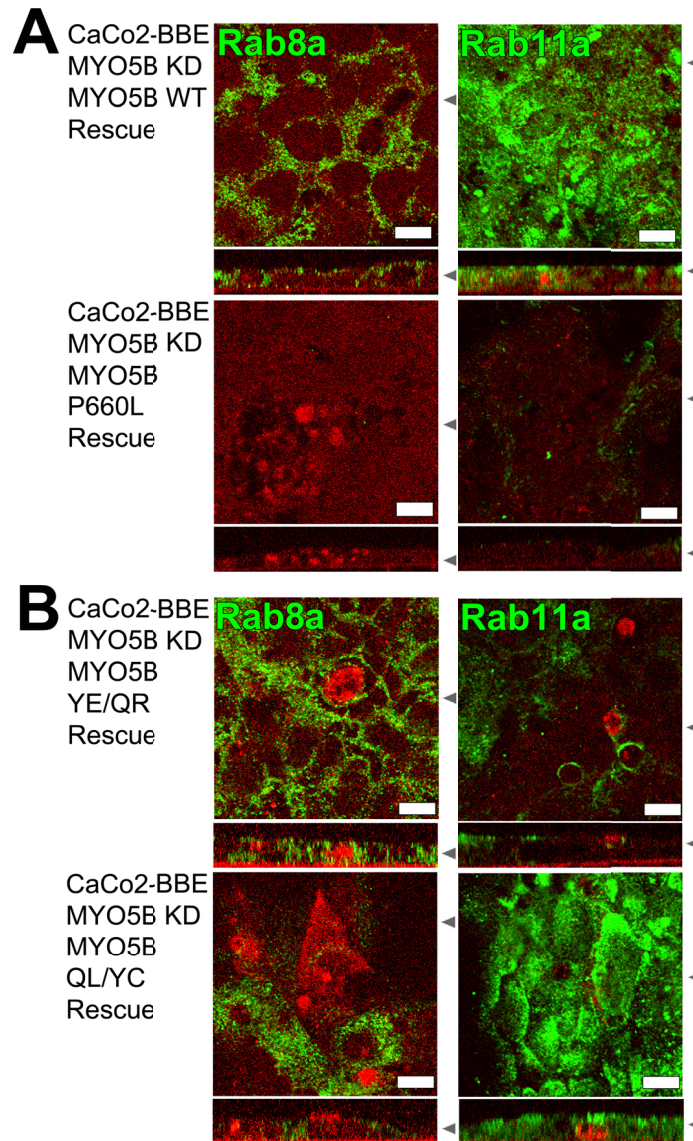
Supplemental Figure 9. Both Rab8a and Rab11a are dispersed from their normal subapical distributions in MVID patient duodenum. (A) Normal duodenum stained for Rab8a showed sub-apical-lateral localization of Rab8a. (B) Staining of MVID patient duodenum for Rab8a showed dispersal of Rab8a and accumulation of Rab8a in small puncta vesicles. (C) Normal duodenum stained for Rab11a showed sub-apical localization of Rab11a. (D) Staining of a MVID patient duodenum for Rab11a showed dispersal from the sub-apical region and accumulation of Rab11a throughout the cytoplasm. It should be noted, for visualization of Rab11a staining in the normal duodenum sample levels were adjusted independently of the MVID patient sample, because of the intense Rab11a staining in the patient sample. Scale bars are 10 μ m in all panels.



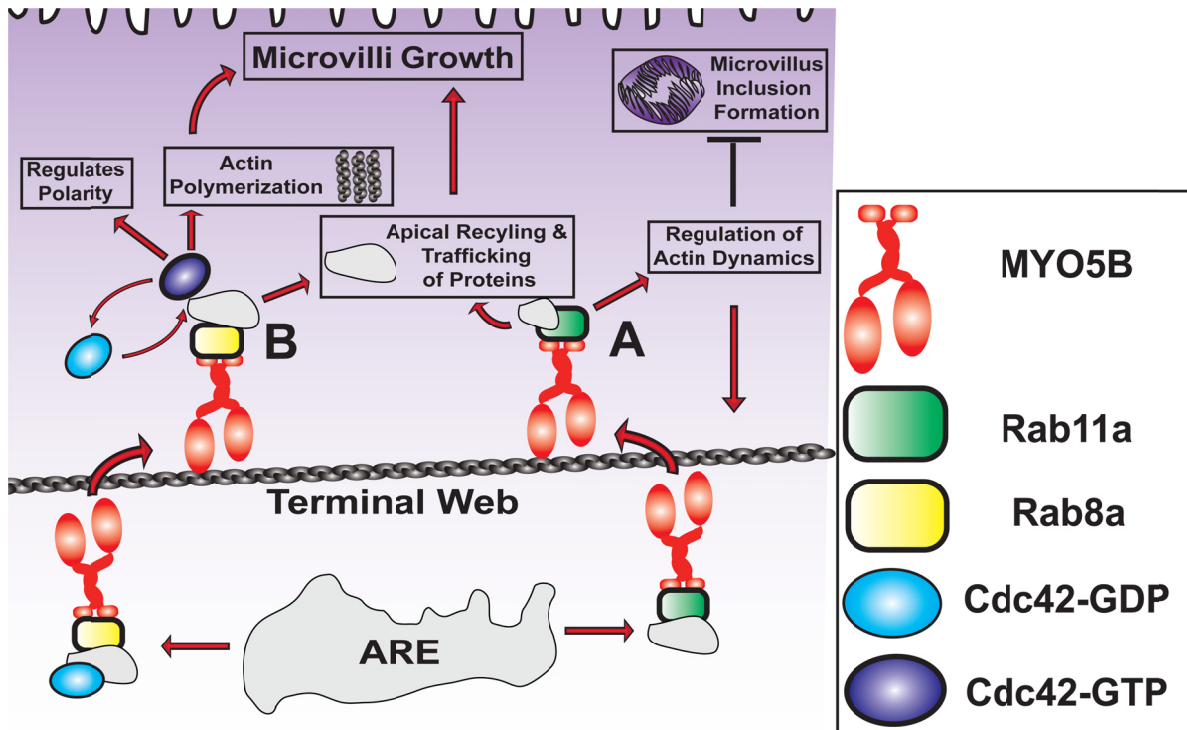
Supplemental Figure 11. Single molecule TIRF-FRAP imaging showed an increase in photo-bleaching in 3x-mCitrine-MYO5B-P660L-1016X transfected constructs compared to 3x-mCitrine-MYO5B-WT-1016X, and these molecules are also stalled on filopodia. (A) Stills of BF16 cells transfected with 3x-mCitrine-MYO5B-WT-1016x or 3x-mCitrine-MYO5B-P660L-1016x and mCherry-Espin over 2 seconds showing localization and movement of 3x-mCitrine-MYO5B-WT-1016x to the tips of filopodia (arrows). 3x-mCitrine-MYO5B-P660L-1016x, however, does not localize to the tips of filopodia and is never observed in active forward motion along F-actin filaments (arrows). Scale bars are 10 μ m. (B) TIRF-FRAP of 3x-mCitrine-MYO5B-WT-1016x (black) and 3x-mCitrine-MYO5B-P660L-1016x (red) showed a greater than 30% increase in photo-bleaching in the 3x-mCitrine-MYO5B-P660L-1016x transfected cells. Error bars denote S.D.



Supplemental Figure 12. Re-expression of MYO5B-WT and MYO5B-P660L in CaCo2-BBE MYO5B-KD cells stained with CLDN1, CLDN2, and DPPIV. In all panels, X-Y confocal images are shown above Z-axis reconstructions. (A) Top: MYO5B-KD cells with mCherry-MYO5B-WT re-expression showed partial recovery of normal CLDN1 and CLDN2 staining. Bottom: MYO5B-KD cells with mCherry-MYO5B-P660L expression showed exacerbation of the MYO5B-KD phenotype with internalization of CLDN1 and an increase in lateral CLDN2 staining. (B) It should be noted, for visualization of DPPIV staining in the mCherry-MYO5B-WT and mCherry-MYO5B-P660L expressing cells were adjusted independently. Top: MYO5B-KD cells with mCherry-MYO5B-WT re-expression showed recovery of normal DPPIV staining. Bottom: MYO5B-KD cells with mCherry-MYO5B-P660L expression showed exacerbation of the MYO5B-KD phenotype with DPPIV positive microvillus inclusion formation. Scale bars are 10µm in all panels.



Supplemental Figure 13. Rab8a and Rab11a immunostaining in MYO5B-KD cells expressing MYO5B-WT rescued Rab8a and Rab11a, MYO5B-QLYC rescued Rab11a, MYO5B-YEQR rescued Rab8a, and MYO5B-P660L does not rescue either Rab. (A) Left-top: Expression of mCherry-MYO5B-WT (red) rescued the dispersal of Rab8a (green) in MYO5B-KD. Left-bottom: Expression of mCherry-MYO5B-P660L (red) failed to rescue the dispersal of Rab8a (green) in MYO5B-KD cells. Right-top: Expression of mCherry-MYO5B-WT (red) rescued the dispersal of Rab11a (green) in MYO5B-KD. Right-bottom: Re-expression of mCherry-MYO5B-P660L (red) failed to rescue the dispersal of Rab11a (green) in MYO5B-KD. (B) Left-top: Expression of mCherry-MYO5B-YE/QR (red) in MYO5B-KD cells rescued Rab8a (green). Left-bottom: Expression of mCherry-MYO5B-QL/YC (red) in MYO5B-KD cells did not rescue Rab8a. Right-top: Expression of mCherry-MYO5B-YE/QR (red) in MYO5B-KD cells did not rescue Rab11a (green). Left-bottom: Expression of mCherry-MYO5B-QL/YC (red) in MYO5B-KD cells rescued Rab11a. In all panels, X-Y confocal images are shown above Z-axis reconstructions. Scale bars are 10 μ m in all panels.



Supplemental Figure 14. MYO5B interacts with Rab8a and Rab11a to regulate enterocyte polarity, apical trafficking, and microvilli growth. The gradient shown attempts to illustrate in white (microtubule rich region) and purple (actin rich region). Both Rab8a and Rab11a bind to MYO5B directly on the ARE. (A) Rab11a regulates actin dynamics in a MYO5B-dependent manner, and has been shown to facilitate apical trafficking and recycling. We have demonstrated in this study that Rab11a is needed to halt microvillus inclusion formation, via actin dependent macropinocytosis. (B) Rab8a plays a role in apical recycling and trafficking, and has also been shown to activate Cdc42 via Tuba, which regulates cellular polarity, and facilitates actin polymerization. All of these together aid in microvilli growth.

Supplemental Video 1. BF16 cells transfected with 3x-mCitrine-MYO5B-WT-1016X (green) and mCherry-Espin (red). Note the movement of 3x-mCitrine-MYO5B-WT-1016X to the tips of filopodia highlighted with mCherry-Espin.

Supplemental Video 2. BF16 cells transfected with 3x-mCitrine-MYO5B-P660L-1016X(green) and mCherry-Espin (red). Note that there is little or no movement of 3x-mCitrine-MYO5B-P660L-1016X to the tips of filopodia highlighted with mCherry-Espin.

Supplemental Table 1. Antibodies used. ND=Not determined.

Antibody	CaCo2-IF Antibody Dilution	Human Tissue - IF Antibody Dilution	Western Blot Antibody Dilution
Active cdc42 ewEast #26905	1:100	ND	ND
aPKC (rabbit) Gift from the Macara Laboratory	1:200	1:200	ND
CD10 Abcam #ab47721-100	1:100	1:100	ND
CD71 Invitrogen #13-6800	1:200	1:200	ND
CDC42 Cell signaling # 2462	1:200	1:200	1:250
Claudin-1 Invitrogen #51-9000	1:200	1:200	1:2000
Claudin-2 Invitrogen #51-6100	1:100	ND	1:1000
Claudin-4 Invitrogen #532-9400	1:100	1:200	1:1000
DPPIV abcam #ab129060	ND	ND	1:1000
DPPIV R&D systems #1180-SE	1:100	1:200	1:500
Ds-Red Clontech #632496	ND	ND	1:2000
E-Cadherin BD # 610181	1:300	ND	1:5000
E-Cadherin Cell Signaling # #3195S	ND	ND	1:1000
Ezrin Cell Signaling #3145	1:200	1:200	1:5000
LAMP2a Abcam #ab18528	1:200	ND	ND
MYO5B (VU410-Chicken) Produced by the Goldenring Laboratory	1:200	1:200	1:1000
Na/K-ATPase Milipore #05-369	1:50	1:50	1:1000
NHE3 (rabbit) Gift from the Ghishan Laboratory	1:400	1:200	ND
p120 BD Transduction Lab # 610133	1:200	1:200	1:2000

p120 (6H11 & FlαSH) Gift from the Reynolds Laboratory	ND	ND	1:1000
Rab11a (8H10- Mouse) Produced by the Goldenring Laboratory	1:200	1:200	ND
Rab11a (VU57- Rabbit) Produced by the Goldenring Laboratory	1:200	1:200	1:2500
Rab8a-AP (Rabbit) Produced by the Goldenring Laboratory	1:200	1:200	1:1000
SGLT1 Abcam #ab14685	ND	1:200	ND
SNX18 Sigma Prestige #HPA037800	1:200	1:200	ND
VDAC-1 Abcam #ab15895			
Villin-1 Cell signaling # 2369	1:100	1:100	1:5000
ZO-1 Invitrogen #61- 7300	1:200	1:200	1:1000
α-Tubulin Cell Signaling #2144	1:200	1:200	1:5000
β-Actin Sigma-Aldrich #A5316	ND	1:200	1:2000
β-Catenin Cell Signaling #9562	1:200	1:200	ND